Two-step K^+–Na^+ and Ag^+–Na^+ ion-exchanged glass waveguides for C-band applications

Jizuo Zou, Feng Zhao, and Ray T. Chen

A two-step K^+–Na^+ and Ag^+–Na^+ ion-exchange technique is introduced to fabricate single-mode channel waveguides in BK7 glass for the telecom-wavelength region. The dependencies of insertion loss, polarization-dependent loss (PDL), and bending loss of curved waveguides on channel width, diffusion time, and annealing time are investigated. Results show that postannealing is a required process for improving waveguide properties and an optimal annealing time exists. Although relatively narrow mask openings are used in most one-step ion-exchange processes, a wider channel width, to as wide as 10 μm, is preferred for this two-step method. The minimum coupling loss to/from single-mode fiber and the propagation loss is found to be 0.4 dB and 0.3 dB/cm, respectively. For 5-cm-long waveguides the PDL is less than 0.1 dB. For the S-bend structure the cosine curve exhibits apparently a lower bending loss than the double-arc curve.

OCIS codes: 230.7380, 130.3120.

1. Introduction

Ion exchange has been considered one of the most important techniques for glass waveguide fabrication for integrated optical devices, such as wavelength division multiplexer/demultiplexer, the power splitter/combiner, and the optical filter. The propagation and the coupling losses of single mode fibers (SMFs) are two challenging issues of ion-exchanged waveguides. One of the most attractive methods in recent years is the two-step K^+–Na^+ and Ag^+–Na^+ ion-exchange approach for SMF-compatible waveguide fabrication.[1,2] During the first ion-exchange step, bare glass wafers are dipped into a pure KNO_3 melt to conduct the K^+–Na^+ ion exchange. The Na^+ ions in the surface region of the glass will be interchanged by the K^+ ions from the KNO_3 melt through thermal diffusion. The K^+ ions will cause a higher refractive index than the Na^+ ions. The ion-exchange temperature and the time of this step must be chosen to make sure that the depth and the refractive-index increase in the K^+ ionic layer are not large enough to support any waveguide mode. After the first ion-exchange step, a standard photolithography process is applied to constructing masking patterns on the glass wafers. Then we immerse these glass wafers into an $AgNO_3$ melt to perform the Ag^+–Na^+ ion exchange. In fact, during the first step, the K^+–Na^+ ion exchange is not complete; a small percentage of the Na^+ ions is left in the K^+ layer. Therefore the Ag^+ ions can diffuse into the glass in the unmasked regions through the K^+ layer. Usually the temperature during the second step is much lower than that of the first step, at which the diffusivity of the K^+ ions is very low; thus the K^+ ionic layer does not change during this step. Because the Ag^+ ions cause a much higher refractive-index increase than the K^+ ions, the index peak is actually below the K^+ ionic layer. As a result, buried waveguides are obtained.

This two-step ion exchange has a few advantages over the one-step Ag^+–Na^+ ion-exchange approach. First, burying the waveguides reduces the scattering and absorption losses induced by the colloidal silver particles that are formed under the edges of the metal mask[3] (usually Al). Second, the waveguide-mode profile is more circular, which matches the SMF better. Third, this two-step process has less side diffusion,[1] which necessitates wider mask openings for SMF-compatible waveguide fabrication. The advantages of the two-step method reported therein are also obvious compared with the commonly used two-step Ag^+–Na^+ and Na^+–Na^+ electric-field-assisted

The authors are with Microelectronics Research Center, J. J. Pickle Research Campus, The University of Texas at Austin, 10100 Burnet Road, Austin, Texas 78758 (e-mail for R. Chen is raychen@uts.cc.utexas.edu).

Received 7 March 2002; revised manuscript received 26 August 2002.

0003-6935/02/367620-07$15.00/0

waveguide burial method.[4] In the electric-field burial process, both complex facilities and complex procedures are required in handling the high voltage at high temperature with molten $NaNO_3$ as the electrodes. From the application point of view these complexities eventually limit the manufacturability. In addition the side diffusion is still a problem. On the other hand the two-step K^+–Na^+ and Ag^+–Na^+ ion-exchange process reported in this paper is almost as simple as the one-step Ag^+–Na^+ method, because there is no special setup or process required in the first step. The weak point of the two-step K^+–Na^+ and Ag^+–Na^+ process is its limited burial depth, which limits the effectiveness of the propagation-loss reduction by waveguide burying.

The theoretical model of this two-step diffusion method was described in Ref. 2, and further experimental results based on this model in Corning 0211 glass are reported in Refs. 1 and 5. Although the advantages of this two-step method have been shown experimentally and clearly in these studies, some important information is still lacking, such as the optimal channel (mask) width, the minimum radius of curvature of the waveguide bend, polarization-dependent loss (PDL), and the annealing influences of these specifications.

For ion-exchanged single-mode waveguide fabrication, two kinds of glass are commonly used owing to their relatively low sodium concentration: Corning 0211 and Schott BK7. For mass production of photonic devices, Schott BK7 is a better choice, since it has more uniform compositions and better optical qualities. In this paper we report our detailed experimental studies of the two-step K^+–Na^+ and Ag^+–Na^+ ion-exchange method in making SMF-compatible optical waveguides centered at wavelengths of 1.55 μm. The studies include propagation loss, coupling loss, PDL and bending loss, and their dependencies on the mask width, annealing time, and diffusion time of the second ion-exchange step.

2. Waveguide Fabrication and Characterization

The ion-exchange procedure was carried out in a crucible furnace with temperature control accuracy of ±1 °C. All the chemicals were contained in stainless-steel beakers. In the first ion-exchange step, precleaned bare BK7 glass wafers without masking were immersed into a pure KNO_3 melt at 400 °C. After 80 min these wafers were pulled out and cooled in air. Then 200-nm-thick aluminum films were deposited on these BK7 wafers, and standard photolithography procedures were applied to construct the masking patterns of the channel waveguide on them. In the second step the masked glass wafers were dipped into a molten mixture of $AgNO_3$:$NaNO_3$ (mole ratio, 0.1:1) at 320 °C for different diffusion times. After the diffusion steps the aluminum films were etched away and all the wafers were cut to a length of 5 cm with both endfaces finely polished.

After the K^+–Na^+ diffusion process the refractive-index profile of the K^+ layer is a complementary error function erf$c(x/d)$ with depth $d = (D_e t)^{1/2}$. Here t is the diffusion time and D_e is the effective diffusion coefficient, which is an Arrhenius type function of temperature[5]:

$$D_e = C_1 \exp(-C_2/T), \tag{1}$$

where T is the absolute temperature and C_1 and C_2 are constants. However, there is no D_e value reported for the K^+–Na^+ ion exchange in BK7 glass at 400 °C. We can estimate D_e by interpolation by using known values of other temperatures. From Ref. 4 D_e is 0.0852 μm^2/min at 385 °C. From Ref. 6 at a temperature of 440 °C and diffusion time of 5 h, d equals 11.66 μm for TE polarization and 10.52 μm for TM polarization. If we take the average of these two polarizations for our case, D_e can be calculated to be 0.408 μm^2/min. By interpolation with Eq. (1) at 400 °C, D_e is 0.134 μm^2/min. For a diffusion time of 80 min, diffusion depth d equals 3.3 μm. Although the data above are for a wavelength of 633 nm, they should not change much if we apply a wavelength of 1.55 μm. This depth of the K^+ ionic layer of BK7 would not support any waveguide mode, and thus the guided mode can be confined only by the Ag^+ region formed during the second ion-exchange step. During the Ag^+–Na^+ ion-exchange step a diluted $AgNO_3$ melt ($AgNO_3$:$NaNO_3$ = 0.1:1 mol) was used instead of a pure $AgNO_3$ melt because a lower Ag^+ concentration can reduce the chance of silver colloid forming on the glass surface and under the edges of the Al mask. The temperature of the second step was 320 °C, just a bit higher than the melting point of $NaNO_3$ (307 °C) but much lower than that of the first step (400 °C).

Both straight channel waveguides and curved channel waveguides have been designed. The straight channels have eight groups with channel widths from 4 to 11 μm with 1-μm increments. Curved channels have both double-arc S-bends and

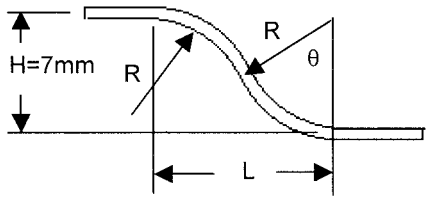

Fig. 1. Double-arc S-bend structure. (The cosine bend has the same H, L values.)

Table 1. Specifications of the Waveguide Bend

R (mm)	L (mm)	H/L	Double-Arc Bends Angle θ (°)	Cosine Bends Minimum Curvature (mm)
5	9.5	0.73	72.5	2.6
10	15.2	0.46	49.5	6.7
15	19.3	0.36	40	10.7
20	22.6	0.31	34.4	14.8
25	25.5	0.27	30.7	18.8
30	28.1	0.25	28	22.9

cosine-function S-bends. Each of them has six groups. For the double-arc bends the six groups correspond to the radii of curvature from 5 to 30 mm with an increment of 5 mm. To compare the bending losses of the cosine bends with the double-arc bends, each of the six cosine-bend groups has the same height H and length L as the double-arc counterparts. H has a fixed value of 7 mm. The bending structure and the specifications are shown in Fig. 1 and Table 1, respectively. The six double-arc groups are denoted by R5, R10, R15, R20, R25, and R30 with the numbers as the radii of curvature in units of millimeter. The same denotation is also used for the cosine group that has the same H and L values as the double-arc one. In total five samples were fabricated. The fabrication conditions are summarized in Table 2.

Even with a diluted $AgNO_3$ melt, metallic silver can still be formed during the second ion-exchange step. In addition, after waveguide fabrication, we found that the waveguide-mode profile is much smaller than that of the SMF. (Detailed results are in Section 3.) Therefore thermal annealing was performed to improve the waveguide properties. During the annealing process the metallic silver particles can diffuse into the glass and change into Ag^+ ions by which propagation loss can be reduced. In the mean time, further diffusion of the Ag^+ ions in the glass will enlarge the mode profile to match the SMF better. The annealing temperature was fixed at 300 °C at which the concentration profiles of the K^+ ions would not change much, while the concentration of the Ag^+ ions will redistribute. The waveguides were characterized after every 12 h of annealing.

The characterization of the waveguides was carried out with the Newport AutoAlign Packaging system shown in Fig. 2. The light source is a broadband laser diode module with a wavelength range of 1.53–1.61 μm. Both the input and the output fibers were attached to a computer-controlled stage with linear positioning accuracy of 0.05 μm. The input and output stages can be controlled to scan along both the lateral X and the vertical Y directions to find the optimal coupling positions between the fiber and the waveguide. A microscope at the top was used as a monitor to keep a minimum gap between the end-faces of the fiber and the waveguide. This can eliminate most of the Fresnel loss.

To obtain the total insertion loss of the waveguide,

Table 2. Fabrication Conditions of the Samples

Sample	Waveguide Pattern	First-Step Time (K^+–Na^+) (min)	Second-Step Time (Ag^+–Na^+)
S1	Straight, Arc S-bends	80	4 h 15 min
S2	Cosine S-bends	80	4 h 15 min
S3	Straight, Arc S-bends	80	5 h
S4	Cosine S-bends	80	5 h
S5	Straight	80	7.5 h

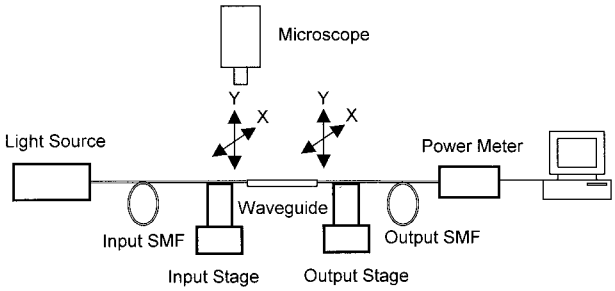

Fig. 2. Waveguide-characterization setup.

the SMF (Corning SM-28) was used as both the input and the output to get power P_{SMF} (dBm). If P_0(dBm) is the power from the input SMF, the insertion loss L_I (dB) is

$$L_I = P_0 - P_{\mathrm{SMF}}. \tag{2}$$

To get the coupling loss between the waveguide and the SMF, the output SMF was changed with a multimode fiber (MMF) with the same SMF as the input. Assume that the measured power is P_{MMF} (dBm), then the coupling loss L_C (dB) is defined as

$$L_C = P_{\mathrm{MMF}} - P_{\mathrm{SMF}}. \tag{3}$$

The propagation loss L_P (dB/cm) is thus determined to be

$$L_P = (L_I - 2{*}L_C)/l, \tag{4}$$

where l(cm) is the waveguide length.

The polarization-dependent loss is the maximum variation of insertion loss over all polarization states. Owing to measurement difficulties, we use the loss difference between the TM and the TE state as the definition of the PDL in our experiment. It was obtained by using a polarization-maintaining fiber with an in-line polarizer as the input with a regular SMF as the output. Once power was obtained for the TM polarization, the input fiber was rotated 90° to get the power of the TE polarization.

3. Results and Discussions

A. Straight Channel Waveguides

By scanning the output SMF along the X and Y directions, we can monitor the waveguide-mode dimensions. The scanning profile is actually the convolution between the waveguide mode and the SMF mode. As a reference the profile obtained by coupling two SMF directly is also obtained. To achieve the best coupling efficiency between the waveguide and the SMF, the scanning profile of the waveguide should be identical to that of the SMF in both the X and the Y directions. From the measured results, all the profiles can fit well with the Gaussian function. The FWHM of the scanning profiles of the channels in S3 before annealing are shown in Fig. 3. We see that the modes of the waveguides are all smaller than that of the SMF. This clearly indicates a low side diffusion and a high refractive-index in-

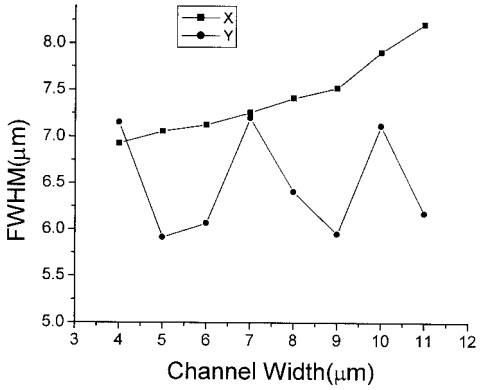

Fig. 3. FWHM of S3 scanning profiles before the annealing.

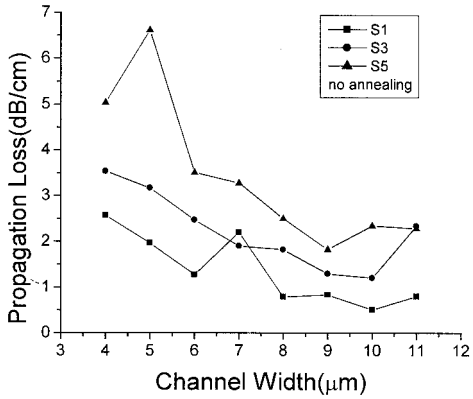

Fig. 4. Propagation losses before the annealing.

crease. In the X direction the FWHM increases monotonously with the channel width. In the Y direction. However, the dependence of the FWHM on the channel width fluctuates strongly. This may be due to contamination of the glass surface by metallic silver particles formed during the second ion-exchange step. Comparing the FWHM data of the X direction with the Y direction, we can find that the narrower channels have more circular mode profiles than the wider channels. For different second-step diffusion times the FWHM of various channels are summarized in Table 3. In the X direction, for the same channel width, the mode size in S1 exhibits no apparent difference from that in S3 or S5. That is, the mode size is not sensitive to the diffusion time.

The propagation and coupling losses of the straight channels before annealing are shown in Figs. 4 and 5. Apparently the propagation loss is the dominant factor in the total insertion loss. After the waveguide fabrication we checked the channels under the microscope and found clear white lines at the channel edges, clearly indicating the metallic silver colloid. These silver lines are buried under the glass surface since they could not be removed by nitric acid. This phenomenon has also been reported in one-step Ag^+–Na^+ ion-exchanged waveguides.[3] These atomic silver particles introduce propagation losses by both absorption and scattering. Figure 4 also shows that the waveguides with longer diffusion time in the second ion-exchange step have higher propagation losses. Under a microscope, we noted that the white silver colloid lines at the channel edges in S1 are smoother than those in S5. It implies that the longer the second-step diffusion time, the more irregularities on the diffusion boundaries.

These irregularities consequently cause higher scattering losses. However, both the amount and the distribution of the metallic silver in the glass are unknown. Another phenomenon in Fig. 4 is that in the same diffusion conditions the wider channels have much lower propagation losses than the narrower channels. In practice, a Gaussian approximation can be applied to both the refractive-index distribution and the mode profile with good accuracy. When the channel width W increases, the full width of the electric-field mode profile ξ will increase at a relatively lower rate, approximately proportional to $\sqrt{W}$.[7] Consequently the normalized magnitude of the electric field at the scatters (silver colloidal lines) $\exp[-(W/\xi)^2]$ will decrease. Therefore, when the channel width increases, the silver particles cause lower absorption and scattering loss. The coupling loss is determined by the mismatch between the waveguide mode and the SMF mode. Owing to less side diffusion and burial of the waveguide mode, the symmetric mode field in X and Y can be obtained. For example, the 7-μm channel has the same full width along the X and Y directions. Then the coupling loss is mainly determined by the mode-size mismatch. Owing to smaller waveguide modes compared with the SMF mode, the coupling losses are

Table 3. Scanning Profile FWHM before Annealing

Channel Width (μm)	Sample S1 (μm)		Sample S3 (μm)		Sample S5 (μm)	
	X	Y	X	Y	X	Y
4	7.2	6.1	6.9	7.1	6.9	6.7
8	7.6	6.8	7.4	6.4	7.5	5.9
10	7.9	5.8	7.9	7.1	8.0	6.7

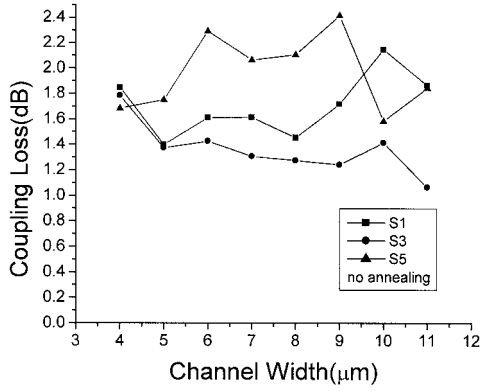

Fig. 5. Coupling losses before the annealing.

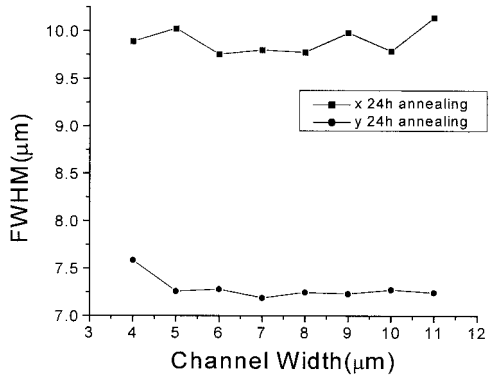

Fig. 6. FWHM of S3 scanning profiles after 24 h of annealing.

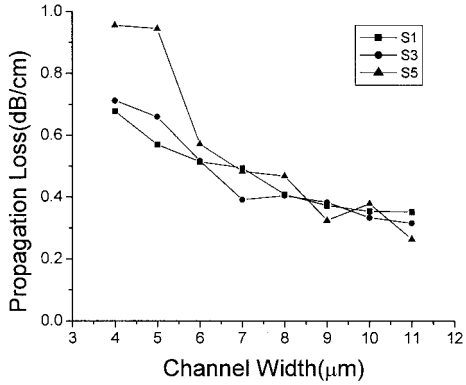

Fig. 7. Propagation losses after the final annealing.

pretty high. As shown in Fig. 5 the resulting coupling losses are between 1 and 2.4 dB for samples S1, S3, and S5. However, from the total insertion loss point of view, the small mode size is not a drawback, because the waveguide must be annealed to reduce propagation losses and the guided mode will be enlarged during the annealing process. The desirable process should give the highest coupling efficiency after a certain interval of thermal annealing instead of just after the ion-exchange step, since the lowest propagation losses can be achieved at the same time.

The annealing process was continued until the coupling loss no longer decreased. The final annealing time was 48 h for S1 and S2 and 24 h for S3, S4, and S5. The FWHM of the scanning profiles of the waveguides in S3 after 24 h of annealing is given in Fig. 6. Compared with Fig. 3, the mode profiles have been significantly enlarged and the fluctuation in the Y direction has been evened out. During annealing the width of the Ag^+ distribution profile along the Y direction increases more slowly than that along the X direction and the mode becomes more elliptical. As shown in Fig. 6 the FWHM does not change much over different channel widths, which means that the thermal annealing plays a more important role in determining the Ag^+ distribution than the initial ion-exchange process. By deconvolution between the scanning profiles and the SMF mode profile, the waveguide mode size (full width at $1/e^2$ of peak intensity) can be calculated to be 13.3 μm along the X direction and 7.0 μm along the Y direction. The measured propagation losses and coupling losses of S1, S3, and S5 after final annealing are given in Figs. 7 and 8. Comparing Figs. 4 and 5, we conclude that both the propagation and the coupling losses have been significantly reduced by thermal annealing. Although S1 and S3 do not show much difference in propagation loss and coupling loss, some narrow channels (4 and 5 μm) of S5 have very large deviations from other channels in these values. Therefore the influence of colloidal silver on these channels in S5 is too severe to be removed by annealing. After annealing the wider channels still have much lower propagation losses than the narrower channels. Quantitatively in the S3 batch the lowest coupling loss and the lowest propagation loss are ~0.4 dB and 0.3 dB/cm, respectively.

After comparing the results after different annealing times, we found that the annealing effect is more significant during the first 12 h of annealing than during the second 12 h of annealing. For example, for the waveguides in S3 the 90% reduction in the propagation loss and 80% reduction in the coupling loss were achieved during the first 12 h, whereas the next 12 h produced much fewer changes.

We changed the launching condition by offsetting the input SMF along both the X and Y directions to evaluate the existence of higher-order modes. Before the annealing, the waveguides in the three samples, S1, S3, and S5, were all single mode. However, after 24 h of annealing, channels wider than 7 μm in S1 and S3 and channels wider than 6 μm in S5 are multimode. Compared with S5, the higher-order modes of the channels in S1 and S3 are more difficult to excite. Therefore the second-step diffusion time should be no longer than 5 h to prevent the appearance of higher-order modes.

The PDL can also be reduced significantly by annealing. The PDLs of the channels in sample S3 with different annealing times are in Fig. 9. The coupling losses have also been monitored for both the TE and TM modes and they were the same. Therefore the PDL mainly came from the propagation loss. Similar to the propagation loss, the PDL was reduced

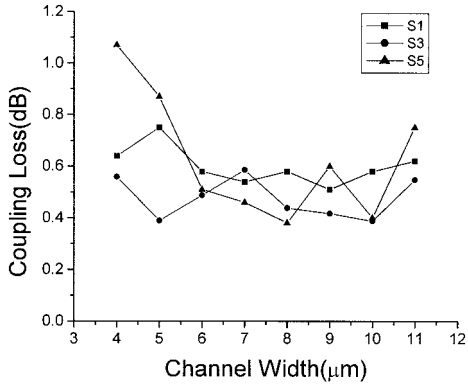

Fig. 8. Coupling losses after the final annealing.

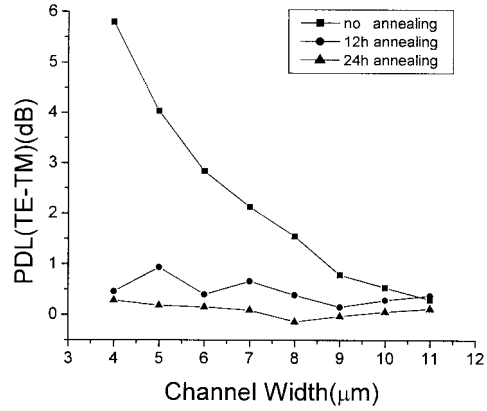

Fig. 9. PDL of S3 with different annealing times.

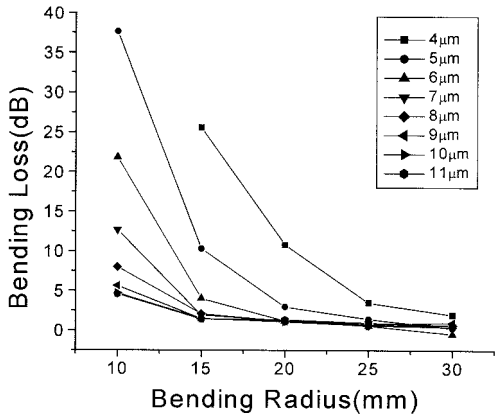

Fig. 10. Bending losses of S3 (arc bends) after 24 h of the annealing.

primarily during the first 12 h of annealing. However, before annealing, the PDLs of the wider channels (such as 11 μm) were already very low, while the propagation losses were not. The final absolute PDL values of sample S3 after 24 h of annealing are less than 0.1 dB.

B. Bending Waveguides

The bending-related parameters of optical waveguides are crucial in integrated optics, because these properties directly determine the integration density. Usually the S-bend is the most commonly used bending structure. Mach–Zehnder interferometers, directional couplers, or power splitters/combiners are examples. Some general information on ion-exchanged glass waveguide bends has been available.[7,8] A comparison of the bending losses of S-bends defined by different functions including linear, circular, cosine, sine, and a kind of polynomial can be found in Ref. 7. For sharp bending the cosine curve has a minimum total bending loss, while for slow bending the polynomial curve is the best. Since we are looking for the highest waveguide bending, we choose a cosine function as our S-bend layout structure in investigating the bending features of the two-step ion-exchanged waveguides in BK7 glass. As a comparison, double-arc curves have also been fabricated.

In an S-bend there are two kinds of losses occurring from the bending, i.e., the straight to/from curve transition loss and the bend radiation loss. The calculation formulas of these two kinds of losses based on a Gaussian approximation are given in Ref. 7. These two bending-related losses are both functions of the radius of curvature R and the waveguide normalized frequency V. With a Gaussian approximation, V is defined as

$$V = K_0 * Q * (2 n_s * \Delta n_m)^{1/2}, \tag{5}$$

where K_0 is the wave number in vacuum and Δn_m and n_s are the peak index increase and the substrate index, respectively, Q is the half-width of the index profile at a 1/e maximum. In our case the waveguides in sample S3 after 24 h of annealing are near the single-mode cutoff region; then V should be close to ~2.4.[9] The largest transition loss calculated is ~0.1 dB for the R5 group. That is, the transition loss is negligible compared with the radiation bend loss (see Figs. 10 and 11). For a given R the radiation loss decreases exponentially with V. Therefore, to lower the bending losses, a larger V number is preferred as long as it is in the single-mode region.

The bending losses are obtained by deducting the straight channel propagation losses from the S-bend propagation losses, including the length correction. Figure 10 and 11 present the bending losses of double-arc bends in sample S3 and cosine bends in sample S4 after 24 h of annealing. The bending loss decreases exponentially versus the radius of curvature. In Fig. 10 the point of 4 μm in the R10 group is missed because the loss is so high that the output is already beyond the detective limit of the power meter. The data for the entire R5 group are also like this. Clearly, the cosine bends have much lower bending loss than the double-arc bends, and the advantages are more remarkable for the smaller bending radii of curvature. For example, in the R10 group the 10-μm channel of a double-arc bend has a higher loss of 2.10 dB than the cosine bend, which corresponds to 1.2 dB/rad. This advantage is especially important when we are trying to scale down our device dimen-

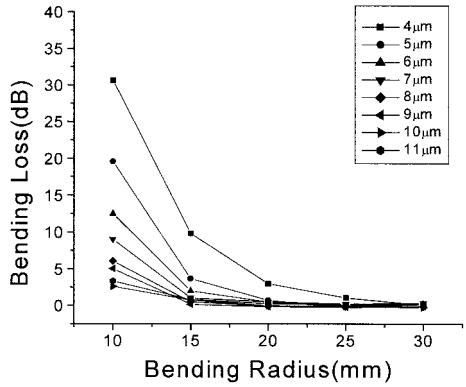

Fig. 11. Bending losses of S4 (cosine bends) after 24 h of the annealing.

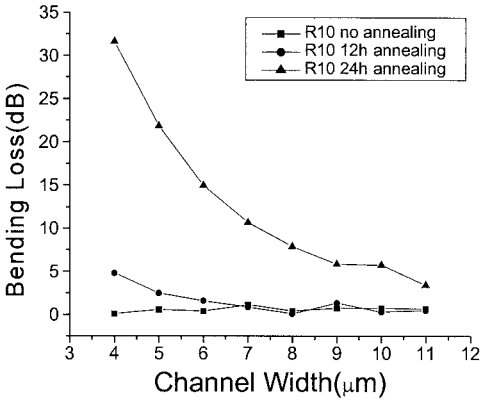

Fig. 12. Bending losses of R10 in S4 with different annealing times.

sions. Another feature is that for both the double-arc bends and cosine bends, the narrower channels always have higher bending losses; this is clearly due to the *V*-number change versus channel widths.

The bending losses can also be affected by thermal annealing. When the waveguide is annealed, the waveguide mode will become larger and the mode confinement will be worse. As a result the bending losses will be increased. The annealing effects on the bending losses of R10 group in sample S4 are shown in Fig. 12. The bending losses are increased dramatically during the second 12 h of annealing, and the narrower channels are more sensitive to the annealing time. That is, from the bending loss point of view a larger channel width is also preferred.

4. Conclusion

Two-step K^+–Na^+ and Ag^+–Na^+ ion-exchanged channel waveguides in BK7 glass have been fabricated and characterized at a wavelength of 1.55 μm. During the first step a pure KNO_3 melt was used at 400 °C to form a planar layer, while during the second step a mixture of $AgNO_3$:$NaNO_3$ (molar ratio, 0.1:1) was used at 320 °C for different times to define the channel waveguide region. After the fabrication, thermal annealing was performed at 300 °C. We have found that before thermal annealing the propagation losses and the PDL are both very high owing to the metallic silver formation under the edge of the Al mask. In the mean time the relatively lower side diffusion effect has been proved. This results in smaller waveguide modes than that of SMF, giving low coupling efficiency to SMF. However, after thermal annealing, all these losses are reduced significantly. After 24 h of annealing the propagation loss of the 11-μm channel in a sample with 5 h of a second-step ion-exchange time has been reduced from 1.2 to 0.3 dB/cm. For this sample a coupling loss to SMF has been reduced from 1.4 to 0.4 dB and the PDL from 0.5 to 0.1 dB (5 cm long). For these losses, most improvements are achieved during the first 12 h of annealing. To prevent the appearance of higher-order modes, the second-step ion-exchange time should be no longer than 5 h. For the same fabrication conditions the wider channels generally have a lower propagation loss and PDL than the narrower channels. However, the coupling loss does not depend much on the channel width. Note that during the first 12 h of annealing the PDL has been reduced more efficiently than the propagation loss.

The bending feature is another topic in our study. Both double-arc S-bends and cosine-function S-bends with different radii of curvature have been studied. From the quantitative results of the bending losses of these S-bends the advantages of the cosine-function bends have been verified. The effects of annealing on bending losses have also been investigated. When thermal annealing is employed, the bending radiation losses will increase. However, this increase is pronounced only after the first 12 h of annealing. In addition, after thermal annealing the bending losses become more sensitive to the channel widths, especially for the narrower channels.

In summary, we concluded that to fabricate SMF-compatible optical waveguides with low insertion losses, low PDL and low bending losses by the two-step K^+–Na^+ and Ag^+–Na^+ ion exchange in BK7 glass, a wider channel width to as great as 10 μm is preferred. In addition the post thermal annealing is required. The propagation losses, coupling losses, and PDL can be significantly reduced during the first 12 h of annealing at 300 °C. On the other hand, for the curved channels the bending losses are increased rapidly after 12 h of annealing. For practical applications the optimal annealing time should be a trade-off determined by the device structure, i.e., whether the structure consists of straight channels, curved channels, or both.

References

1. M.-J. Li, S. Honkanen, W.-J. Wang, S. I. Najafi, A. Tervonen, and P. Pöyhönen, "Buried glass waveguides by ion-exchange through an ionic barrier," in *Micro-Optics II*, A. M. Scheggi, ed., Proc. SPIE **1506,** 52–57 (1991).
2. A. Tervonen and S. Honkanen, "Model for waveguide fabrication in glass by a two-step ion exchange with ionic masking," Opt. Lett. **13,** 71–73 (1988).
3. R. G. Walker and C. D. W. Wilkinson, "Integrated optical waveguiding structures made by silver ion exchange in glass. 1. the propagation characteristics of stripe ion-exchanged waveguides: a theoretical and experimental investigation." Appl. Opt. **22,** 1923–1928 (1983).
4. S. I. Najafi, *Introduction to Glass Integrated Optics* (Artech House, Boston, 1992).
5. W. J. Wang, S. Honkanen, and S. I. Najafi, "Loss characteristics of potassium and silver double-ion-exchanged glass waveguides," J. Appl. Phys. **74,** 1529–1533 (1993).
6. C. Ciminelli, A. D'Orazio, M. De Sario, C. Gerardi, V. Petruzzelli, and F. Prudenzano, "Effects of thermal annealing on the optical characteristics of K^+–Na^+ waveguides," Appl. Opt. **37,** 2346–2356 (1998).
7. H. F. Schlaak, A. Branderburg, and G. Sulz, "Integrated optical circuits with curved waveguides," in *Integrated Optical Circuit Engineering III*, R. T. Kersten, ed., Proc. SPIE **651,** 38–45 (1986).
8. R. G. Walker and C. D. W. Wilkinson, "Integrated optical waveguiding structures made by silver ion exchange in glass. 2. Directional coupler and bends," Appl. Opt. **22,** 1929–1936 (1983).
9. H.-G. Unger, *Planar Optical Waveguides and Fibers* (Clarendon, Oxford, UK, 1977).